MAT 280: Laplacian Eigenfunctions: Theory, Applications, and Computations
Lecture 15: Use of Laplacian Eigenfunctions and Eigenvalues for Analyzing Data on a Domain of Complicated Shape

Lecturer: Naoki Saito
Scribe: Lawrence Austria/Allen Xue

May 23, 2007

This lecture is based on [1] and [2].

1 Motivation

Consider a bounded domain of general shape $\Omega \subset \mathbb{R}^d$. The region Ω maybe as simple as a rectangular domain in $\mathbb{R}^2$, or as complicated as a map of an island or a retinal ganglion cell of a mouse; see Figure 1.

We wish to analyze the spatial frequency inside of the object defined in Ω, at the same time, we need to avoid the Gibbs phenomenon due to the boundary $\Gamma = \partial\Omega$. We also want to represent the object information efficiently for analysis, interpretation, and discrimination; this includes examining fast decaying expansion coefficients relative to a meaningful basis. Further, we want to extract geometric information about the domain Ω. For more details, see [1], [2].

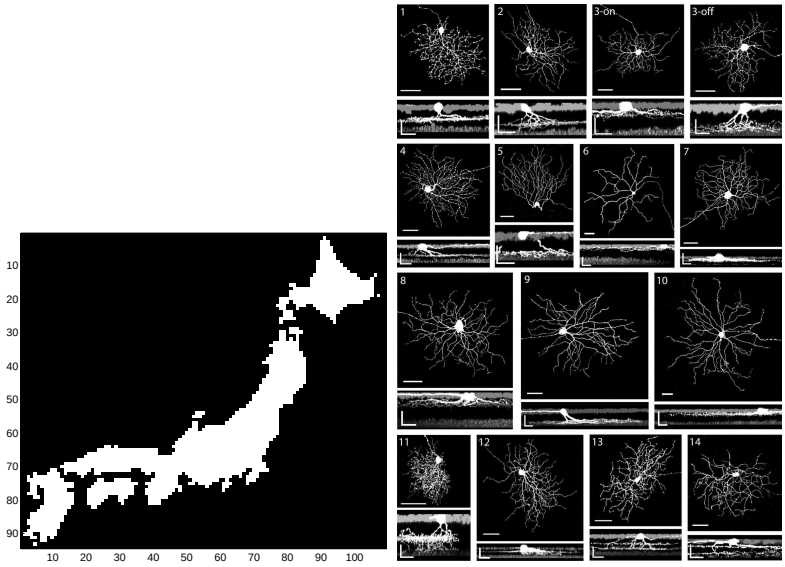

(a) (b)

Figure 1: Complicated Domains.

2 Laplacian Eigenfunctions

Our previous attempt was to extend the object to the outside smoothly and then bound it nicely with a rectangular box followed by the ordinary Fourier analysis. Because various domains give rise to different sets of Laplacian eigenfunctions, it makes sense to analyze (and synthesize) the object using genuine basis functions tailored to the domain. For instance, *sines* (and *cosines*) are eigenfunctions of the Laplacian on the rectangular domain with Dirichlet (and Neumann) boundary condition. Also *Spherical harmonics, Bessel functions*, and *Prolate Spheroidal wave functions*, are part of the eigenfunctions of the Laplacian (via separation of variables) for the *spherical, cylindrical*, and *spheroidal* domains, respectively.

2.1 Difficulties

Consider the operator $\mathcal{L} = -\Delta$ in $L^2(\Omega)$ with an appropriate boundary condition. In the case when Ω is simple, e.g., a bounded interval $(a, b) \subset \mathbb{R}$, or a rectangular region in $\mathbb{R}^d$, analysis of $\mathcal{L}$ is relatively straightforward. In general, however, analysis of $\mathcal{L}$ is difficult mainly due to its unboundedness. On the other hand, it

is much better to analyze its inverse, i.e., the Green's operator because it is **compact** and **self-adjoint**. Thus $\mathcal{L}^{-1}$ has discrete spectra (i.e., countable number of eigenvalues with finite multiplicity) except for the 0 spectrum. We use the fact that $\mathcal{L}$ induces a complete orthonormal basis for $L^2(\Omega)$ to allow us to perform **eigenfunction expansion** in $L^2(\Omega)$. Another difficulty is computing such eigenfunctions; directly solving the Helmholtz equation (or the Laplacian eigenvalue problem) on a general domain Ω is tough. In addition, computing the Green's function for a general Ω satisfying the usual boundary conditions (e.g., Dirichlet or Neumann) is very difficult too.

3 Integral Operators Commuting with the Laplacian

Instead of computing the eigenfunctions of $\mathcal{L}$ on a general domain, we look at certain integral operators **commuting** with $\mathcal{L}$. The key idea is to find an integral operator commuting with the Laplacian without imposing the strict boundary condition a priori. Then we know that the eigenfunctions of the Laplacian is the same as those of the integral operator, which is much easier to deal with–thanks to the following fact:

Theorem 3.1 (G. Frobenius 1878?; B. Friedman 1956)**.** *Suppose $\mathcal{K}$ and $\mathcal{L}$ commute and one of them has an eigenvalue with finite multiplicity. Then $\mathcal{K}$ and $\mathcal{L}$ share the same eigenfunction corresponding to that eigenvalue. That is, $\mathcal{L}\varphi = \lambda\varphi$ and $\mathcal{K}\varphi = \mu\varphi$.*

Now, let's replace the Green's function $G(\boldsymbol{x}, \boldsymbol{y})$ by the **fundamental solution of the Laplacian**:

$$K(\boldsymbol{x}, \boldsymbol{y}) = \begin{cases} -\frac{1}{2}|x - y| & \text{for} \quad d = 1 \\ -\frac{1}{2\pi} \log |\boldsymbol{x} - \boldsymbol{y}| & \text{for} \quad d = 2 \\ \frac{1}{(d-2)\omega_d} |\boldsymbol{x} - \boldsymbol{y}|^{2-d} & \text{for} \quad d > 2 \end{cases}$$

where ω_d is the surface area of the d-dimensional unit ball. The price we pay is to have a rather implicit, **non-local** boundary condition (although we do not need to deal with this condition directly). Let $\mathcal{K}$ be the integral operator whose kernel is K, i.e., for all $f \in L^2(\Omega)$, define:

$$\mathcal{K}(f(\boldsymbol{x})) \triangleq \int_\Omega K(\boldsymbol{x},\boldsymbol{y}) f(\boldsymbol{y})\,\mathrm{d}\boldsymbol{y}.$$

On the other hand, what we gain are the following:

Theorem 3.2. *The integral operator $\mathcal{K}$ commutes with the Laplacian $\mathcal{L} = -\Delta$ with the following non-local boundary condition:*

$$\int_\Gamma K(\boldsymbol{x},\boldsymbol{y}) \frac{\partial \varphi}{\partial \nu_{\boldsymbol{y}}}(\boldsymbol{y})\,\mathrm{d}s(\boldsymbol{y}) = -\frac{1}{2}\varphi(\boldsymbol{x}) + \mathrm{pv}\int_\Gamma \frac{\partial K(\boldsymbol{x},\boldsymbol{y})}{\partial \nu_{\boldsymbol{y}}}\varphi(\boldsymbol{y})\,\mathrm{d}s(\boldsymbol{y})$$

for all $\boldsymbol{x} \in \Gamma = \partial\Omega$, where φ is an eigenfunction common for both operators.

Corollary 3.3. *The integral operator $\mathcal{K}$ is compact and self-adjoint in $L^2(\Omega)$. Thus the kernel $K(\boldsymbol{x},\boldsymbol{y})$ had the following eigenfunction expansion (in the sense of mean convergence):*

$$K(\boldsymbol{x},\boldsymbol{y}) \sim \sum_{j=1}^{\infty} \mu_j \varphi_j(\boldsymbol{x})\overline{\varphi_j(\boldsymbol{y})}$$

and $\{\varphi_j\}_{j=1}^{\infty}$ forms an orthonormal basis of $L^2(\Omega)$

3.1 Examples

Example 3.4. Consider the simplest example, when $\Omega = (0,1) \subset \mathbb{R}$. Then our integral operator $\mathcal{K}$ with the kernel $K(x,y) = -\frac{1}{2}|x-y|$ gives rise to the eigenvalue problem:

$$\begin{cases} -\varphi'' = \lambda\varphi \text{ , for } x \in (0,1) & \text{(DE)} \\ \varphi(0) + \varphi(1) = -\varphi'(0) = \varphi'(1) & \text{(BC).} \end{cases}$$

Note that the kernel $K(x,y)$ is of **Toeplitz** form; thus, the eigenvectors must have even and odd symmetry [6]. In this case, we have the following explicit solution (the first 5 eigenfunctions are shown in Figure 2):

- $\lambda_0 \approx -5.756915$, which is a solution of the equation: $\tanh(\frac{\sqrt{-\lambda_0}}{2}) = \frac{2}{\sqrt{-\lambda_0}}$. And the corresponding eigenfunction is

$$\varphi_0(x) = A_0 \cosh(\sqrt{-\lambda_0})\left(x - \frac{1}{2}\right);$$

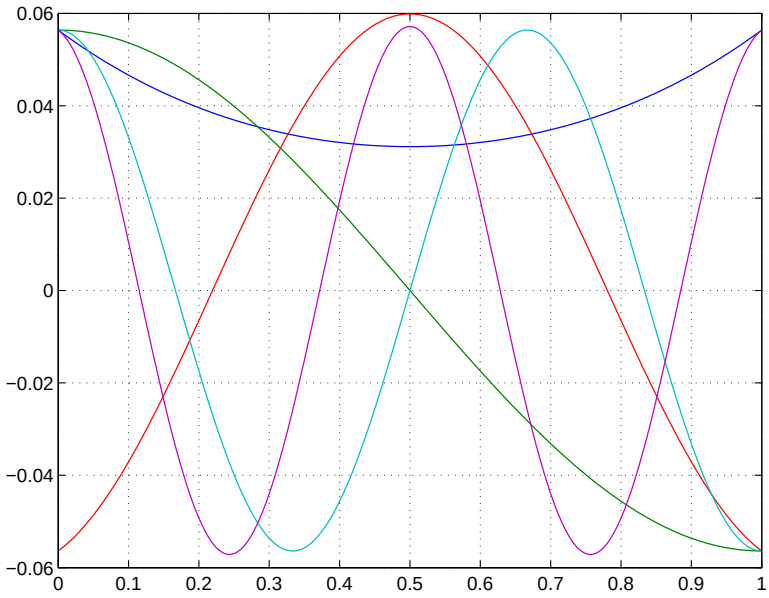

Figure 2: First 5 eigenfunctions.

- $\lambda_{2m-1} = (2m-1)^2\pi^2$ for all $m \in \mathbb{N}$, and the corresponding eigenfunction is

$$\varphi_{2m-1}(x) = \sqrt{2}\cos(2m-1)\pi x;$$

- λ_{2m} for all $m \in \mathbb{N}$ is a solution of the equation: $\tan\frac{\sqrt{\lambda_{2m}}}{2} = -\frac{2}{\sqrt{\lambda_{2m}}}$, and the corresponding eigenfunction is

$$\varphi_{2m}(x) = A_{2m}\cos\sqrt{\lambda_{2m}}\left(x-\frac{1}{2}\right).$$

The constants A_{2m}, $m = 0, 1, 2, \ldots$ are normalization constants to have $\|\varphi_{2m}\| = 1$.

Example 3.5. Now let $\Omega = B(0,1) \subset \mathbb{R}^2$ be the unit disc. Our operator $\mathcal{K}$ with the kernel $K(\boldsymbol{x},\boldsymbol{y}) = -\frac{1}{2\pi}\log|\boldsymbol{x}-\boldsymbol{y}|$, gives rise to the eigenvalue problem:

$$\begin{cases} -\Delta\varphi = \lambda\varphi \text{ , in } \Omega & \text{(DE)} \\ \frac{\partial\varphi}{\partial\nu}\Big|_\Gamma = \frac{\partial\varphi}{\partial r}\Big|_\Gamma = -\frac{\partial\mathcal{H}\varphi}{\partial\theta}\Big|_\Gamma, & \text{(BC)} \end{cases}$$

where $\mathcal{H}$ is the Hilbert transform for the circle:

$$\mathcal{H}f(\theta) \triangleq \frac{1}{2\pi}\text{pv}\int_{-\pi}^{\pi} f(\eta)\cot\frac{\theta-\eta}{2}\,\mathrm{d}\eta$$

for all $\theta \in [-\pi, \pi]$. Now, let $\beta_{k,\ell}$ be the ℓ-th zero of the Bessel function of the first kind of order k, then

$$\varphi_{m,n}(r,\theta) = \begin{cases} J_m(\beta_{m-1,n}r)\cos(m\theta) & \text{for all } m,n \in \mathbb{N} \\ J_m(\beta_{m-1,n}r)\sin(m\theta) & \text{for all } m,n \in \mathbb{N} \\ J_0(\beta_{0,n}r) & \text{if } m = 0, n \in \mathbb{N} \end{cases}$$

$$\lambda_{m,n} = \begin{cases} \beta^2_{m-1,n} & \text{if } m,n \in \mathbb{N} \\ \beta^2_{0,n} & \text{if } m = 0, n \in \mathbb{N} \end{cases}$$

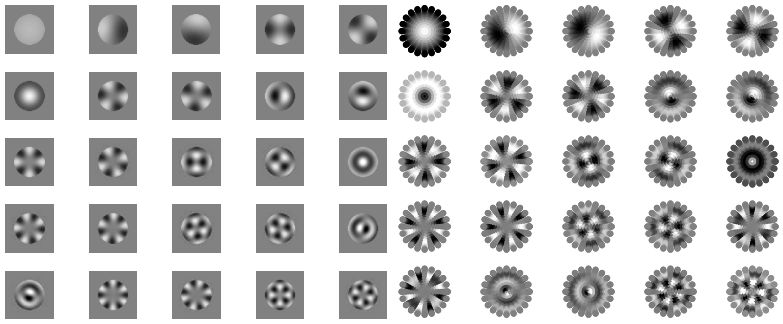

(a) (b)

Figure 3: Left: First 25 eigenfunctions of Our integral operator $\mathcal{K}$; Right: First 25 eigenfunctions of the Dichlet-Laplace via separation of variables.

Example 3.6. Consider the unit ball $\Omega = B(0,1) \subset \mathbb{R}^3$. Then our integral operator uses the kernel:

$$K(\boldsymbol{x},\boldsymbol{y}) = \frac{1}{4\pi|\boldsymbol{x}-\boldsymbol{y}|}.$$

The first 9 eigenfunctions cut at the equator viewed from the south is depicted in Figure 4.

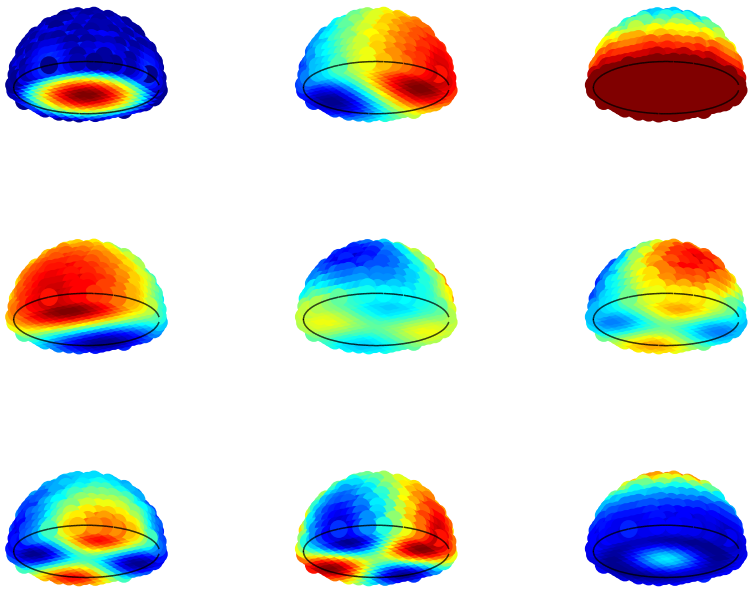

Figure 4: First 9 eigenfunctions cut at the equator viewed from the south.

4 Discretization of the Problem

Assume that the whole data set consists of a collection of data sampled on a rectangular grid, and that each sampling cell is a box of size $\prod_{i=1}^{d} \Delta x_i$. Further, assume that an object of our interest Ω consists of a subset of these boxes whose centers are $\{\boldsymbol{x}_i\}_{i=1}^{N}$. Under these assumptions, we can approximate the integral eigenvalue problem $\mathcal{K}\varphi = \mu\varphi$ with a simple quadrature rule with node-weight pairs $(\boldsymbol{x}_j, w_j)$ as follows:

$$\sum_{j=1}^{N} w_j K(\boldsymbol{x}_i, \boldsymbol{x}_j)\varphi(\boldsymbol{x}_j) = \mu\varphi(\boldsymbol{x}_i)$$

$$w_j = \prod_{k=1}^{d} \Delta x_k$$

for all $1 \leq j \leq N$. Let $K_{i,j} \triangleq w_j K(\boldsymbol{x}_i, \boldsymbol{x}_j)$, $\varphi_i \triangleq \varphi(\boldsymbol{x}_i)$, and $\boldsymbol{\varphi} \triangleq (\varphi_1, \cdots, \varphi_N)^T \in \mathbb{R}^N$. The above equation can be written in a matrix-vector form $K\boldsymbol{\varphi} = \mu\boldsymbol{\varphi}$, where $K = (K_{i,j}) \in \mathbb{R}^{N\times N}$. Under our assumptions, the weight w_j does not depend on j; therefore, K is *symmetric*.

5 Applications

5.1 Image Approximation

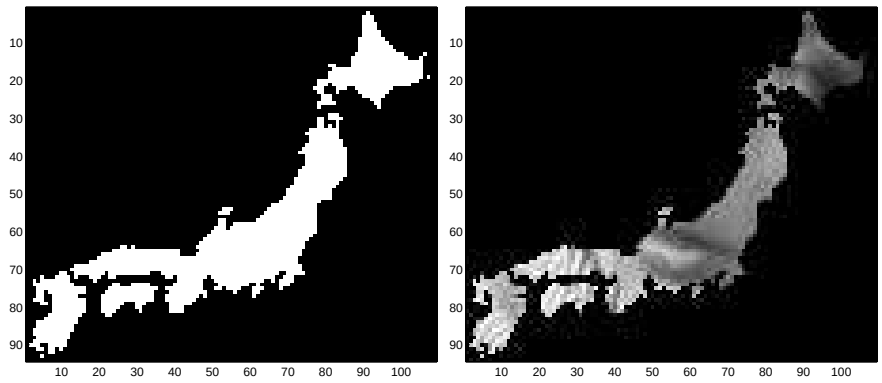

(a) χ_Ω (b) $\chi_\Omega \cdot$ Barbara

Figure 5: The characteristic function of the Japanese Islands (a) and the Barbara image overlaid over the islands.

In this section, we provide a brief summary of the approximation capability of the Laplacian eigenfunction for given image data on an irregularly-shaped domain, and compare the performance with that of the standard wavelet-based methods.

Let Ω be the digitized image of the islands of Japan. We define the characteristic function $\chi_\Omega(\boldsymbol{x})$ to indicate the space of the island. As an example, we form a function (or data) on Ω by multiplying the standard Barbara image with χ_Ω; see Figure 5.

For this particular example, the number of samples forming the data on the island is 1625; therefore, computing the Laplacian eigenfunctions defined on Ω involves a kernel matrix of size 1625×1625.

Figure 6 shows a reconstruction of the data set using the largest 100 coefficients. Figure 7 shows another reconstruction using the largest 100 coefficients computed via the standard 2D wavelet basis called *Symmlet 8*. Notice that the 100 wavelet coefficients cannot even capture the boundary of the domain, not to mention the data on the domain.

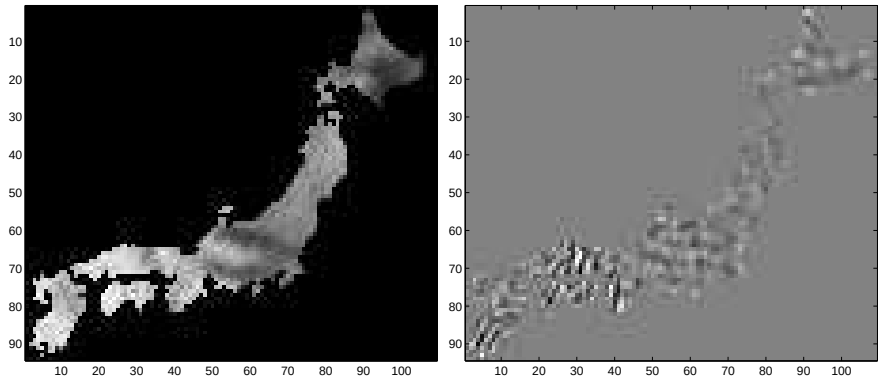

(a) 100-term Approx. (b) Error

Figure 6: The 100-term approximation and the residual error using the Laplacian eigenfunctions.

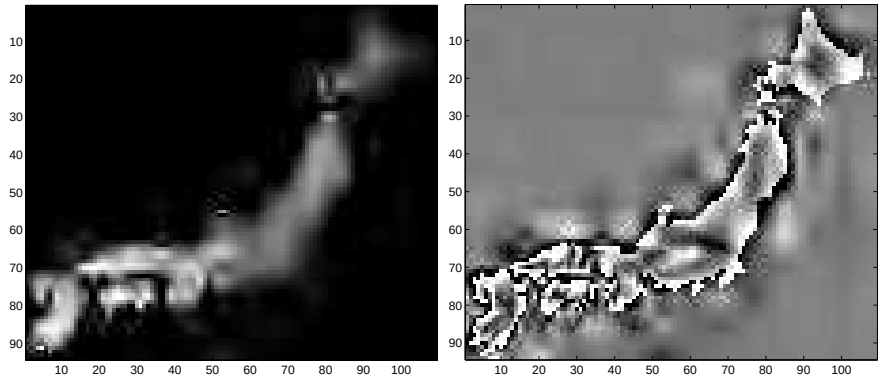

(a) 100-term Approx. (b) Error

Figure 7: The 100-term approximation and the residual error using the 2DWavelets (Symmlet 8).

To be fairer, though, we organize the 1625 data points in a one-dimensional array in a column scanning order. After applying the 1D wavelet transform to this 1D array using the Symmlet 8 filter, we recompute the 100-term approximation and its residual errors, as shown in Figure 8. Observe the stripe-shaped artifacts in the approximation due to the deconstruction of the 2D spatial coherency of the

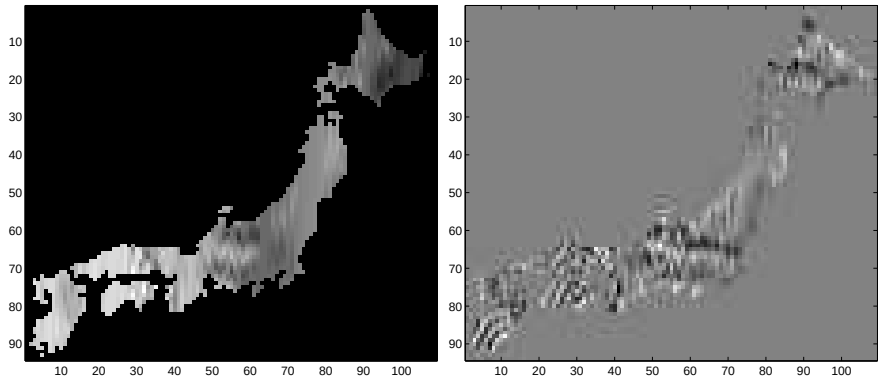

(a) 100-term Approx. (b) Error

Figure 8: The 100-term approximation and the residual error using the 1DWavelets (Symmlet 8).

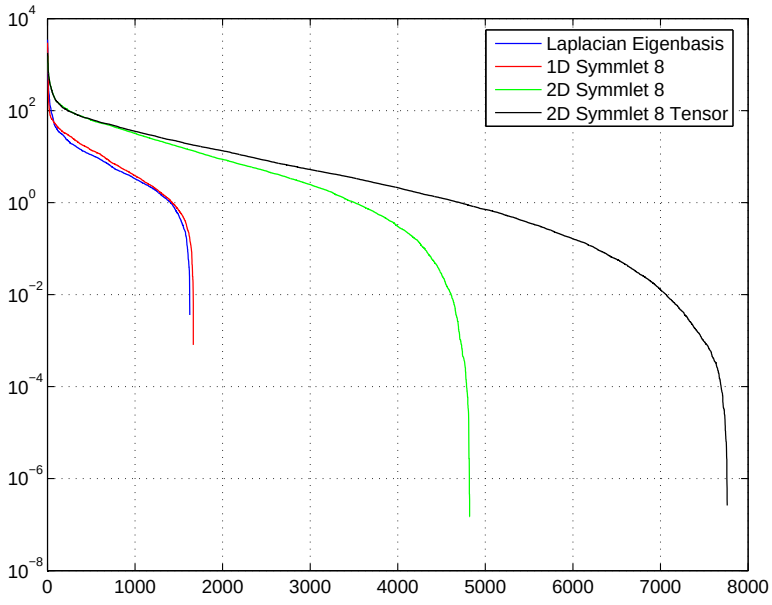

Figure 9: Comparison of the approximation error in ℓ^2 using these transforms.

original data by arranging them into a 1D array.

We conclude this section with the following conjecture, which essentially says that the approximation performance of our eigenfunctions for a general domain is the same order as that of the Fourier cosine series (or DCT) for a rectangular domain:

Conjecture 5.1 (NS 2005)**.** *For $f \in C(\overline{\Omega})$ with $\nabla f \in BV(\overline{\Omega})$ defined on a C^2-domain Ω, the expansion coefficients $\langle f, \varphi_k \rangle$ with respect to the Laplacian eigenbasis decay $O(k^{-1})$. Thus, the N-th approximation error measured in L^2-norm should have a decay rate of $O(N^{-1.5})$.*

5.2 Statistical Image Analysis; Comparison with PCA

See [2, Sec. 5] for the details.

5.3 Solving the Heat Equation on a Complicated Domain

It is well known that the semigroup $\mathrm{e}^{t\Delta}$ can be diagonalized using the Laplacian eigenbasis. More precisely, for any initial heat distribution $u_0(\boldsymbol{x}) \in L^2(\Omega)$, we have the heat distribution at time t formally as:

$$u(\boldsymbol{x}, t) = \mathrm{e}^{t\Delta} u_0 = \sum_{j=1}^{\infty} \mathrm{e}^{-t\lambda_j} \langle u_0, \varphi_j \rangle \varphi_j(\boldsymbol{x})$$

which is based on the expansion of the Green's function for the heat equation $\rho_t(\boldsymbol{x}, \boldsymbol{y})$ via the Laplacian eigenfunctions as follows:

$$\rho_t(\boldsymbol{x}, \boldsymbol{y}) = \sum_{j=1}^{\infty} \mathrm{e}^{-\lambda_j t} \varphi_j(\boldsymbol{x}) \overline{\varphi_j(\boldsymbol{y})}, \quad (t, \boldsymbol{x}, \boldsymbol{y}) \in (0, \infty) \times \overline{\Omega} \times \overline{\Omega}.$$

In practice, the domain Ω is discretized by a finite number (i.e., $N \in \mathbb{N}$) of sample points (or pixels), thus the Laplacian eigenfunctions become the Laplacian eigenvectors of length N. Therefore, we can write $\mathrm{e}^{t\Delta}$ in the matrix-vector notation as

$$\Phi \mathrm{e}^{-t\Lambda} \Phi^T = \Phi \, \mathrm{diag}(\mathrm{e}^{-\lambda_1 t}, \cdots, \mathrm{e}^{-\lambda_N t}) \Phi^T = \sum_{j=1}^{N} \mathrm{e}^{-\lambda_j t} \boldsymbol{\varphi}_j \boldsymbol{\varphi}_j^T$$

where $\Phi = (\boldsymbol{\varphi}_1, \cdots, \boldsymbol{\varphi}_N)$ is the Laplacian eigenbasis matrix of size $N \times N$, and Λ is the diagonal matrix consisting of eigenvalues of the Laplacian, which are the inverse of the eigenvalues of the kernel matrix $K = (K_{i,j})$, i.e., $\Lambda_{k,k} = \lambda_k = \frac{1}{\mu_k}$.

Given an initial heat distribution over the domain, $\boldsymbol{u}_0 \in \mathbb{R}^N$, we can compute the heat distribution at time t as:

$$\boldsymbol{u}(t) = \Phi \mathrm{e}^{-t\Lambda} \Phi^T \boldsymbol{u}_0.$$

Figure 10 shows the result of a simple numerical experiment on the Japanese islands data sets.

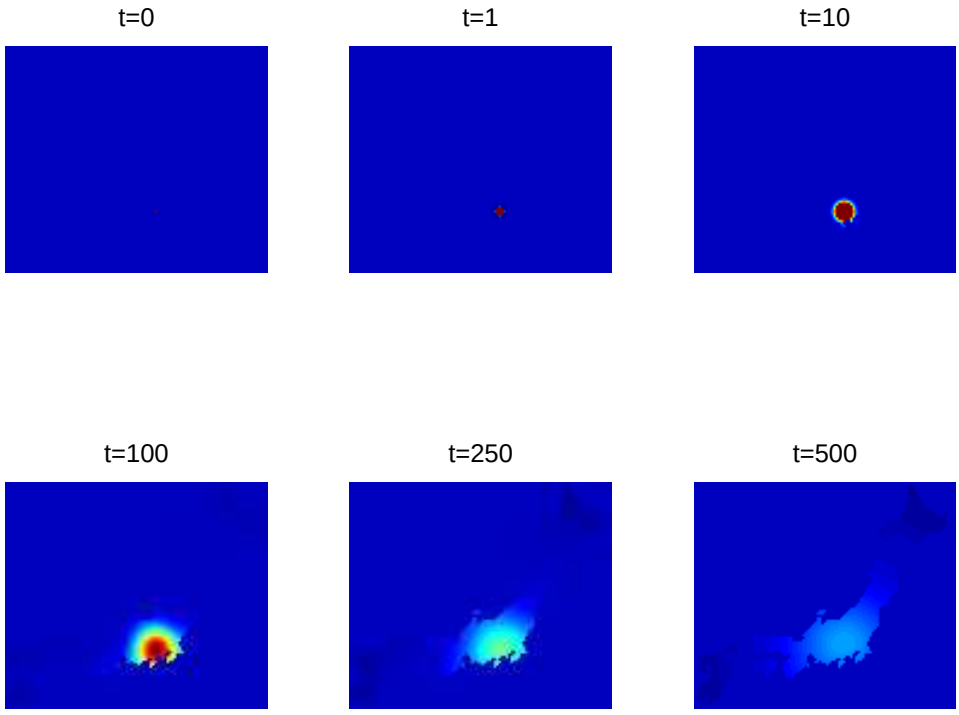

Figure 10: The propagation of the heat distribution over the Japanese Islands. The initial point heat source was put at the location of Mt. Fuji.

To learn more relationships between heat equation and spectral geometry, see [3].

5.4 Clustering Mouse Retinal Ganglion Cells

In this section, we examine how Laplacian eigenfunctions help us understand how the structural/geometric properties of mouse **retinal ganglion cells** (RGCs) re-

late to the cell types and their functionality. For the background of mouse retinal ganglion cell datasets, see [4] and [5]. Our data consists of 3D images of dendrites/axons of RGCs. The process (often arduous) involves examining each images via specialized software to extract geometric/morphological parameters (totally 14 parameters) followed by a conventional (often arduous) clustering algorithm.

The parameters include: somal size, dendric field size, total dendrite length, branch order, and mean internal branch length. Typically, it takes half a day to process each cell with a lot of human interaction.

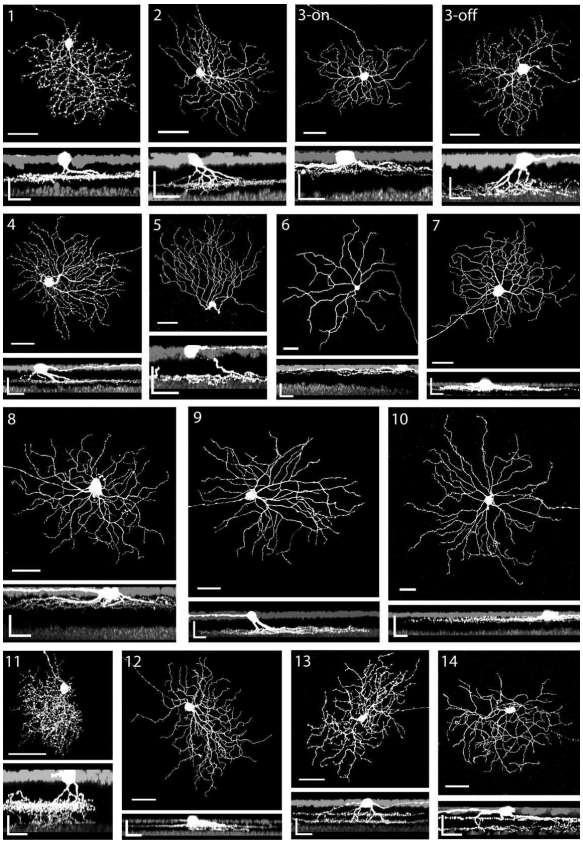

Figure 11: Mouse Retinal Ganglion Cells (plan and side views).

5.4.1 Very Preliminary Studies

Our preliminary study on mouse RGCs consists of 1) using 2D plane projection of the data instead of the full 3D, computing the smallest k Laplacian eigenvalues using our method (i.e., the largest k eigenvalues of K) for each image; 2) constructing a **feature vector** per image; and 3) performing visualization and clustering (see Figure 12). The possible feature vectors reflecting geometric information are:

$$\mathbf{F}_1 = (\lambda_1, \cdots, \lambda_k)^T$$
$$\mathbf{F}_2 = (\mu_1, \cdots, \mu_k)^T$$
$$\mathbf{F}_3 = \left(\frac{\lambda_1}{\lambda_2}, \cdots, \frac{\lambda_1}{\lambda_k}\right)^T$$
$$\mathbf{F}_4 = \left(\frac{\mu_1}{\mu_2}, \cdots, \frac{\mu_1}{\mu_k}\right)^T$$

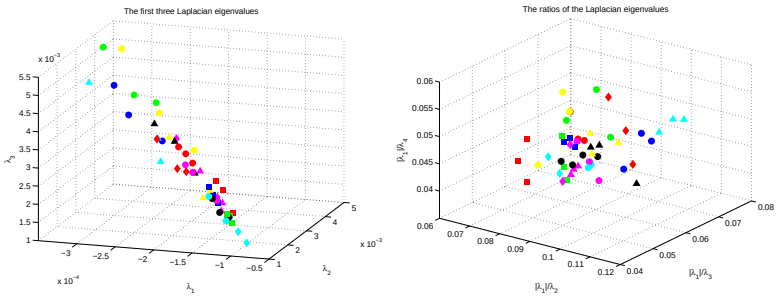

(a) $\boldsymbol{F}_1$ (b) $\boldsymbol{F}_3$

Figure 12: Visualization anc clustering using $\boldsymbol{F}_1$ (a) and $\boldsymbol{F}_3$ (b).

5.4.2 Challenges of the Mouse Retinal Ganglion Cells Problem

The shapes of the RGCs are very complicated. In addition, interpretation of our eigenvalues are not yet fully understood compared to the usual Dirichlet-Laplacian case that have been well studied. Perhaps using the original 3D data may yield a more meaningful result instead of the projected 2D data. Another way to approach this problem is to construct actual graphs based on the connectivity and

analyze them directly via spectral graph theory and diffusion maps (see Lectures 18-20). Lastly, because we are dealing with very complicated domains with many sample points (see Figure 14), we need to develop a faster algorithm to reduce computational burden.

6 A Possible Fast Algorithm For Computing φ_j's

We take advantage of the fact that our kernel function $K(\boldsymbol{x}, \boldsymbol{y})$ is of special form. More precisely, it is the fundamental solution of the Laplacian used in Potential theory. One way to construct a faster algorithm is to accelerate the matrix-vector product $K\boldsymbol{\varphi}$ using the **Fast Multipole Method (FMM)** [7]. We convert the kernel matrix to the tree-structured matrix via FMM whose submatrices are nicely organized in terms of their ranks.

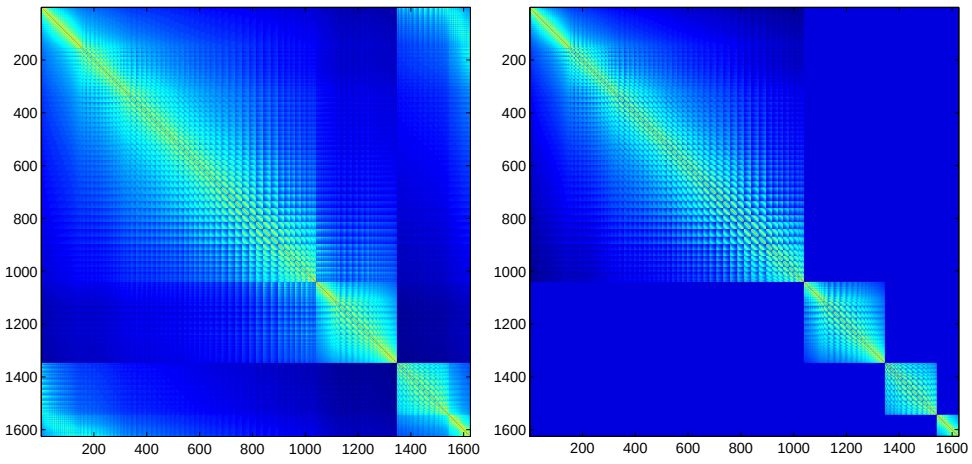

(a) Whole islands (b) Separated islands

Figure 13: The kernel matrix where the communications between and within the islands are kept (a) and the one without in-between communication (b).

Our current implementation cost $O(N \log N)$; Another approach is to construct an $O(N)$ matrix-vector product module fully utilizing **rank** information. For more detailed treatment, see the *HSS* algorithm of Chandrasekaran et al. (2006) [8]. We then embed the matrix-vector product module in the Krylov subspace method, e.g., Lanczos iteration. As a result, the computational cost for each eigenvalue and eigenvector is $O(N)$.

Lastly, if a domain of data support consists of disconnected components, then we can reduce the original problem into a set of smaller problem. For instance, we can separate the Japanese island into four major islands, as shown in Figure 13.

7 Conclusions

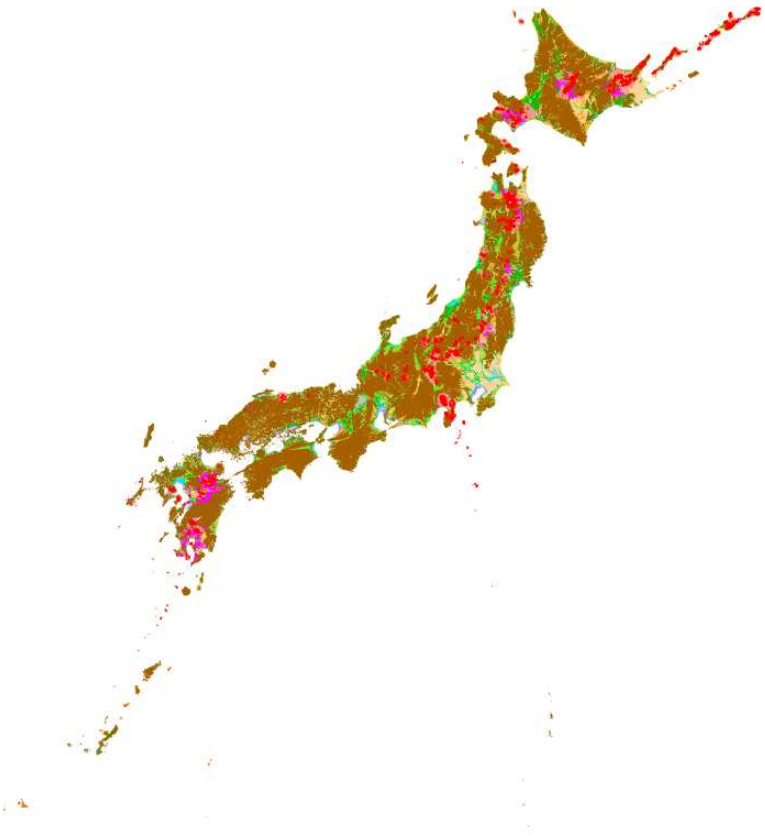

Figure 14: Real Challenge: The number of sampling points in this map is 387,394 over the Japanese Islands.

We demonstrated that our Laplacian eigenfunctions may be useful for object oriented image analysis and synthesis in which the user can define the image domain freely and explicitly with the help of interactive device (e.g., pointer/mouse) or

some automatic segmentation algorithm. We also demonstrated that our method based on the eigenanalysis of the commuting integral operator leads to unconventional non-local boundary condition for the Laplacian eigenvalue problem, but that the numerical implementation is straightforward and is amenable to modern fast algorithms. Our experiments and analogy with the analytic examples suggest that we should be able to get fast-decaying expansion coefficients if the images are in $C(\overline{\Omega})$ and $\nabla f \in \mathrm{BV}(\overline{\Omega})$, where the boundary of Ω is smooth. In essence, our method can be viewed as a replacement of DCT for the general shape domain. This means that our eigenfunctions have a variety of potential applications e.g., interpolation, extrapolation, local feature computation, and perhaps compression. In addition, it connects several interesting mathematics, including spectral geometry, spectral graph theory, isoperimetric inequalities, Toeplitz operators, PDEs, potential theory, and almost-periodic functions.

References

[1] N. SAITO, "Geometric Harmonics as a Statistical Image Processing Tool for Images Defined on Irregularly Shaped Domains," in *Proc. IEEE Workshop on Statistical Image Processing*, Bordeaux, France, Jul. 2005

[2] N. SAITO, "Data Analysis and Representation Using Eigenfunctions of Laplacians on a General Domain," Submitted to *Applied and Computational Harmonic Analysis*, Mar. 2007

[3] J. DODZIUK, "Eigenvalues of the Laplacian and the Heat Equation," *Amer. Math. Monthly*, vol. 88, no. 9, pp. 686-695, 1981.

[4] J, COOMBS, D. VAN DER LIST, G.-Y. WANG, AND L.M. CHALUPA, "Morphological Properties of Mouse Retinal Ganglion Cells", *Neuroscience*, vol. 140, no. 1, pp. 123-136, 2006.

[5] J.-H. KONG, D.R. FISH, R.L. ROCKHILL, AND R.H. MASLAND, "Diversity of Ganglion Cells in the Mouse Retina: Unsupervised Morphological Classification and its Limits", *The Journal of Comparative Neurology*, vol. 489, no. 3, pp. 293-310, 2005.

[6] A. CANTONI, P. BUTLER, "Eigenvalues and eigenvectors of symmetric centrosymmetric matrices", *Linear Algebra Appl.*, vol. 13, pp. 275-288, 1976.

[7] L. GREENGARD, V. ROKHLIN, "A fast algorithm for particle simulations", *J. Comput. Phys.*, vol. 73, pp. 325-348, 1987.

[8] S. CHANDRASEKARAN, M. GU, AND T. PALS, "A fast ULV decomposition solver for hierarchically semi-separable representations", *SIAM J. Matrix Anal. Appl.*, vol. 28, No. 3, pp. 603C622, 2006.